

Modulated Traveling Waves for the Kuramoto–Sivashinsky Equation

Harry S. Brown

Simulation Sciences Inc.
601 South Valencia Ave.
Brea, CA 92621

Ioannis G. Kevrekidis

Department of Chemical Engineering
Princeton University
Princeton, NJ 08544

Abstract. We present a computational study of modulated traveling waves (MTW) and their local and global bifurcations using the Kuramoto–Sivashinsky Equation (KSE) as an illustrative example. An algorithm for the computation and stability analysis of MTW is described and implemented; we describe simple modifications that allow this algorithm to be incorporated in standard continuation/bifurcation software like AUTO. In addition to the bifurcation of MTW branches from both simple traveling waves and from standing waves (limit cycles), the phenomena computationally studied range from the MTW analog of “infinite period” bifurcations to period doubling cascades of MTW.

1 Introduction

Computational studies of the development of spatiotemporal patterns in nonlinear partial differential equations (PDEs) ranging from reaction–diffusion systems to fluid mechanics necessitate algorithms for the accurate calculation of a hierarchy of important solution types. Such solutions involve spatially nonuniform steady states, constant shape traveling waves, as well as various types of both spatially and temporally varying solutions, such as standing (oscillatory, but non-traveling) waves. The purpose of this paper is to describe an algorithm for the systematic computation, continuation and stability analysis of the type of solutions called modulated traveling waves (MTW). These solutions play an important role in the progressive symmetry breaking and development of spatiotemporal chaos, and are observed in a number of models of physical systems (e.g. two dimensional fluid flow Soibelman [1989], Soibelman and Meiron [1991],

1991 *Mathematics Subject Classification.* Primary 35B32, Secondary 65M60, 35K30.

This paper was originally submitted for publication September 16, 1993.

binary fluid convection Knobloch and Moore [1990], axial-flow gas compressors Adomaitis and Abed [1992] and cellular flames (Bayliss et al. [1992, 1993]).

Most theoretical studies of MTWs in the literature have been in the context of fluid flow problems. Rand [1982], motivated by Taylor Couette experiments, uses symmetry arguments to study properties of MTWs, including a proof of the absence of frequency entrainment of MTW and an analysis of super- and sub-critical bifurcations of MTW from traveling waves. In his forthcoming monograph on Couette flow, Iooss [1993] studies the bifurcation behavior of MTWs. Armbruster et al. [1988, 1989] examine MTWs on the center-unstable manifold of the Kuramoto-Sivashinsky Equation. Recently, Bayliss et al. [1992, 1993] presented a careful numerical study of the rich phenomenology of MTWs in cellular flames; they also used phase-amplitude equations to model some of the bifurcations involved.

Our illustrative example will be the Kuramoto-Sivashinsky equation (KSE), a model of interfacial instabilities in thin film flow (Atherton and Homsy [1976], Benney [1966], Sivashinsky and Michelson [1980]). Both the algorithm and the bifurcations studied, however, are applicable to general nonlinear evolution PDEs.

We consider autonomous PDEs with periodic boundary conditions of the form:

$$V_t + F(V; \alpha) = 0, \quad V(x, t) = V(x + 2\pi, t). \quad (1.1)$$

α represents a bifurcation parameter. An MTW is a solution of (1.1) which appears as a limit cycle (“modulated”) in a coordinate frame traveling at the appropriate speed C . $V(x, t)$ will appear as a spatiotemporal oscillation (Figure 1) which after a time interval T , returns to a spatially shifted (“traveling”) version of its initial shape. Because of the existence of two characteristic frequencies (one associated with the periodic boundary conditions, and the other associated with the modulation), they appear in phase space as invariant T^2 tori, and could in principle be computed as such (see Kevrekidis et al. [1985], van Veldhuizen [1987] for example). However, MTW are special types of tori with the property:

$$V(x, t) = V(x + CT, t + T).$$

They are therefore easier to compute than generic T^2 tori since the two frequencies are decoupled from each other. Letting $V(x, t) = U(x + Ct, t)$ and substituting this assumed form of $V(x, t)$ into (1.1) takes the PDE into a moving coordinate frame:

$$U_t + CU_x + F(U; \alpha) = 0. \quad (1.2)$$

If C is chosen correctly, the translational (traveling) motion can be removed and the MTW can then be computed as a limit cycle. Figure 2 shows a phase portrait of an MTW and its underlying limit cycle. The “correct” traveling speed C cannot be found *a priori*, and since it generally changes with the system parameters ($C = C(\alpha)$), it is not possible to directly compute MTW as limit cycles of (1.2) for a given value of α . The algorithm presented here computes C iteratively.

This paper is organized as follows: we begin by describing the basic algorithm and our Fourier spectral (spatial) – shooting (temporal) implementation (section 2). We then briefly introduce the KSE and a few of its scaling properties (section 3). The computational results are then discussed in detail in section 4.

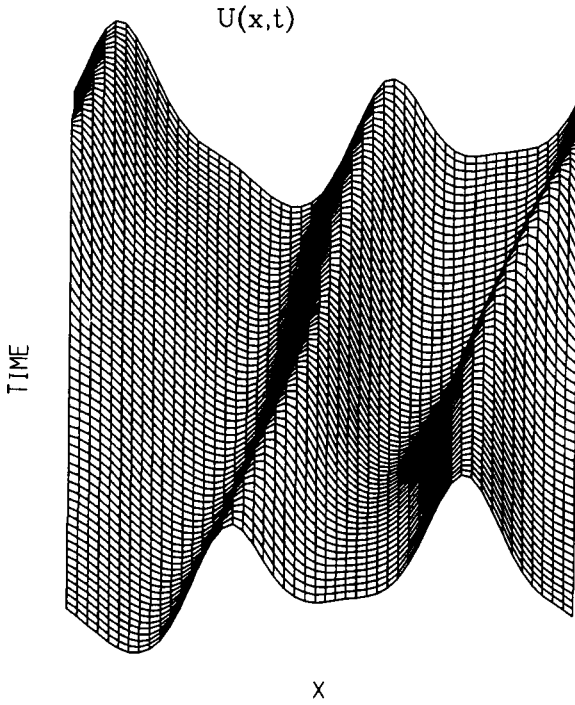


Figure 1 One period of an MTW. This one is stable and occurs at $\alpha = 53.3$.

2 An Algorithm for MTW Computation

Given the form of $F(U; \alpha)$ in equation (1.2), the minimum information needed to describe an MTW is: (a) a point on the torus (an initial condition $U(x)$); (b) the “traveling” speed C ; and (c) the “modulation” period T .

Because of the periodic boundary conditions, we use Fourier spectral spatial discretization of the PDE; the algorithm can, however, be used with other spatial discretization schemes. If U is approximated as the truncated Fourier series:

$$U(x, t) \approx a_0 + \sum_{n=1}^N a_n(t) \cos(nx) + \sum_{n=1}^N a_{n+N}(t) \sin(nx), \quad (2.1)$$

then, after suitable projection (we use Galerkin), a set of $2N + 1 \equiv M$ ordinary differential equations (ODEs) arises from (1.2):

$$\ddot{\vec{a}} = \vec{g}(\vec{a}, C; \alpha). \quad (2.2)$$

To find a limit cycle of a set of M general coupled nonlinear ODEs using a standard shooting method, one iterates on $\vec{a}(t=0)$ and T until:

$$\vec{a}(t=T) - \vec{a}(t=0) \equiv \vec{H}(\vec{a}, t) = 0 \quad (2.3)$$

is satisfied. This represents a system of M algebraic equations in $M + 1$ unknowns. The system (2.3) linearized at a solution is singular since the Jacobian matrix $\frac{\partial \vec{H}(t=T)}{\partial \vec{a}(t=0)}$ has $\frac{\partial \vec{a}}{\partial t}$ as a null vector; this simply reflects the translational invariance in time that all limit cycles possess. The invariance is eliminated, and the system

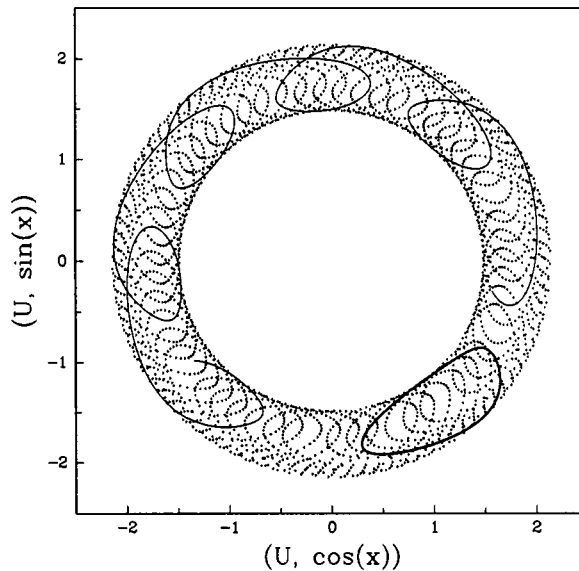


Figure 2 Phase space portrait of the stable MTW at $\alpha = 53.3$. The notation $(U, \cos(x)) \equiv \int_0^{2\pi} U(x, t) \cos(x) dx$ represents the coefficient of $\cos(x)$ in a Fourier series truncation of U . The thin solid curve is a portion of a trajectory on the torus in a stationary coordinate frame ($C = 0$) and the thick solid curve is the trajectory in an appropriately traveling coordinate frame ($C = 48.44055$). In this coordinate frame, the MTW appears as a simple limit cycle. The term “PMPY” (Pushmi-Pullyu!) was used in Bayliss et al. [1993] to describe the characteristic space time evolution of such an MTW.

(2.3) is closed by appending a phase pinning constraint $P(\vec{a}) = 0$. This is now a well posed set of $M + 1$ equations which can be solved via Newton’s method to obtain \vec{a} and T , Doedel [1981], Keller [1976].

For a (temporal) limit cycle of a PDE with spatially periodic boundary conditions, in addition to the translational invariance in t , with its corresponding null vector U_t , arbitrarily shifting the solution in space yields a one parameter family of limit cycles. This is the reason for an additional null vector U_x . Such a family of limit cycles can be thought of as a 2-dimensional surface (a function of x and t) that can be freely translated in x and t . The surface can also be thought of as a T^2 torus in phase space which is invariant under translations in x and t .

Our purpose is to computationally locate this torus. Such a formulation accounts for: (a) one parameter families of standing (nontraveling) waves, parameterized by the spatial shift; (b) MTW, whose trajectories become dense on the surface of the torus when the ratio of the two frequencies, T and $C/2\pi$, is irrational; and (c) MTW with rational frequency ratio, yielding a one parameter family of neutrally stable periodic oscillations on the surface of the torus.

To find a point on the torus (locate the modulated traveling wave), we remove the spatial and temporal shift invariants by appending two pinning conditions and thus closing the shooting equations:

$$\begin{aligned} \vec{a}(t = T) - \vec{a}(t = 0) &\equiv \vec{H} = 0 \\ P_1(\vec{a}) &= P_2(\vec{a}) = 0 \end{aligned} \quad (2.4)$$

P_1 and P_2 are the phase pinning constraints and $\vec{a}(t = T)$ is found by integration of the initial conditions $\vec{a}(t = 0)$. This yields $M + 2$ equations in $M + 2$ unknowns. Assuming good initial guesses, the correct values of $\vec{a}(t = 0)$, C , and T can be found by applying Newton iteration on (2.4). An example of such pinning constraints that we have successfully used was to fix a local extremum of $U(x, t)$ at the point $x = t = 0$. Thus as written in (2.4) $P_1(\vec{a}) \equiv U_x(x = t = 0)$ and $P_2(\vec{a}) \equiv U_t(x = t = 0)$. For the Fourier discretization (2.1):

$$P_1(\vec{a}) \equiv U_x(x = t = 0) = \sum_{n=1}^N n a_{n+N}(t = 0) \quad (2.5)$$

$$P_2(\vec{a}) \equiv U_t(x = t = 0) = \sum_{n=0}^N \dot{a}_n(t = 0). \quad (2.6)$$

To solve (2.4) via Newton's method, one must integrate variational equations to obtain the sensitivities of $\vec{a}(t)$ with respect to the initial conditions $\vec{a}(t = 0)$. Sensitivity with respect to the period T is obtained by evaluating the vectorfield at $t = T$:

$$\frac{\partial U(t = T)}{\partial T} = U_t(t = T) \longrightarrow \frac{\partial \vec{a}(T)}{\partial T} = \dot{\vec{a}}(T)$$

and sensitivity with respect to the speed C is:

$$\frac{\partial U(T)}{\partial C} = \frac{\partial U(x + CT, T)}{\partial C} = T U_x(T).$$

$\frac{\partial \vec{a}(t=T)}{\partial C}$ is easily obtained from this. The partial derivatives of the last two scalar equations in (2.4) can be found by direct differentiation of (2.5) and (2.6); this completes the calculation of the Jacobian matrix of (2.4). A more detailed discussion of this matrix, its relation to the stability of the MTW, and this particular choice of pinning conditions is contained in Appendix A.

A multiple shooting version of this algorithm has been implemented in a pseudo-arclength continuation scheme and the expected quadratic convergence to both stable and unstable MTW was observed.

3 The KSE and its Scaling Law

As an illustrative example for the application of the algorithm described above, we calculate MTW and their bifurcations for the KSE in one spatial dimension:

$$V_t + \frac{\alpha}{2} (V_x)^2 + \alpha V_{xx} + 4V_{xxx} = 0. \quad \text{[Comment icon]}$$

This equation has been derived as a model of spatiotemporal instabilities in a number of physical settings. In the context of thin film flow down an inclined plane, the instability parameter α contains various physical property values of the fluid and is inversely proportional to the square of the length scale over which periodic boundary conditions are applied. Because of α 's dependence on the "spatial box size", the KSE with periodic boundary conditions possesses a replication property allowing new solutions to be inferred from already known solutions at different

values of α . The property is most easily illustrated for the KSE in a moving coordinate frame (speed = C , $U(x, t) = V(x + Ct, t)$):

$$U_t + \frac{\alpha}{2} (U_x)^2 + \alpha U_{xx} + CU_x + 4U_{xxxx} - \frac{\alpha}{4\pi} \int_0^{2\pi} (U_x)^2 dx = 0. \quad (3.1)$$

Replication Law: If $(U(x, t), C; \alpha)$ is a solution of (3.1), with periodic boundary conditions on $x \in [0, 2\pi]$, then $(U(kx, k^4t), k^3C; k^2\alpha)$, where k is any integer, is also a solution.


This law is valid for time dependent as well as steady solutions. It can be used to predict replications of transient solutions, traveling waves, limit cycles, and modulated traveling waves in addition to steady states. For steady states ($C = 0$) the solutions generated with $k = 1, 2, 3, \dots$ are referred to as unimodal, bimodal, trimodal, etc. solutions Kevrekidis et al. [1990], Scovel et al. [1988]. Like steady states, the above law shows that (pure) traveling waves, MTW, and limit cycles (standing waves) will also have k -modal replicas. If a unimodal traveling wave or modulated traveling wave has speed C , then its k -modal replica will travel with speed k^3C . Similarly, if a unimodal MTW or limit cycle has period T , then the period of its k -modal replica will be T/k^4 .


Applying the replication law with $k = -1$ generates information about solutions at the *same* parameter values: if $(U(x, t), C)$ is a solution of the KSE, then $(U(-x, t), -C)$ is also a solution. Spatially even steady states remain invariant under this transformation. When applied to traveling waves and MTW, this transformation yields a right traveling solution from a left traveling one and *vice versa*. Such solutions therefore appear in pairs at the same parameter value.

4 Results for the KSE

The computational results reported here were obtained using a 9 Fourier mode truncation of the KSE ($N = 9$ in equation (2.1)) with full dealiasing. In the regime of α values studied, we believe these results are essentially converged, *i.e.* they remain almost quantitatively unchanged if more Fourier modes are kept in the discretization.

Birth and death of MTW

Figure 3 shows a partial bifurcation diagram of the KSE  comparatively low values of α . The picture (and its blowup around $\alpha = 17$) shows the first (in increasing α) occurrence of an MTW branch. It also illustrates two of the codimension 1 bifurcations involving the birth (death) of an MTW branch: via Hopf (local) bifurcation from a pure traveling wave solution, and via an “infinite period” global bifurcation involving an interaction with a persistent homoclinic connection between steady states. Figure 4 shows how the speed and period of the MTW evolve as homoclinicity is approached.

The basic elements of this diagram —excluding the actual MTW branches— have been discussed in detail elsewhere (e.g. Brown et al. [1991], Kevrekidis et al. [1990]). The uniform (flat) steady state bifurcates to a spatially nonuniform steady state at $\alpha = 4$; this is the unimodal steady state branch. Replicas of both the bifurc n and the branch can be found at $\alpha = 16$ (bimodal steady state branch), $\alpha = 36$ (trimodal branch), etc. Mixed mode steady state branches (like the bi-tri branch seen in the diagram to bifurcate from the bimodal at $\alpha \sim 22.56$) are also

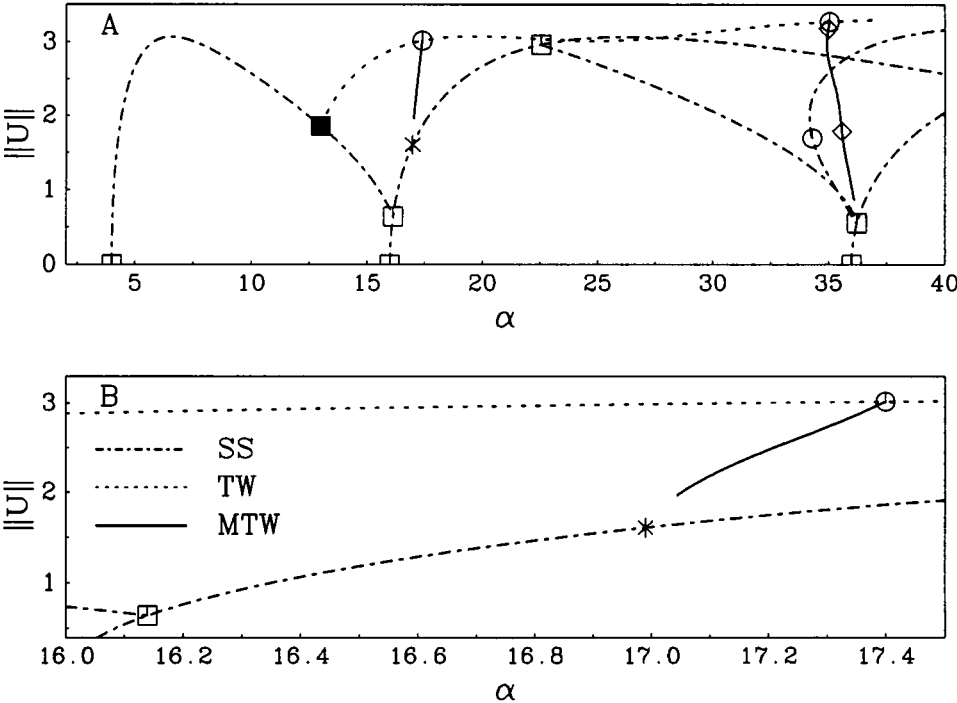


Figure 3 KSE bifurcation diagram showing a subcritical MTW approaching homoclinic connection with bimodal steady states. Stability is not indicated on this graph. The point marked “*” indicates the lowest value of α for which the homoclinic connection is attracting ($\alpha^* = 16.99022$). In this figure, and all that follow, steady states, traveling waves, and modulated traveling waves are abbreviated: “SS”, “TW”, and “MTW” respectively. \circ marks Hopf bifurcation points, \diamond marks period doubling bifurcations, \square marks pitchfork bifurcations, and \blacksquare marks traveling wave bifurcations. The latter is a bifurcation from nontraveling to traveling solutions (steady states \rightarrow traveling waves, or limit cycles \rightarrow MTWs).

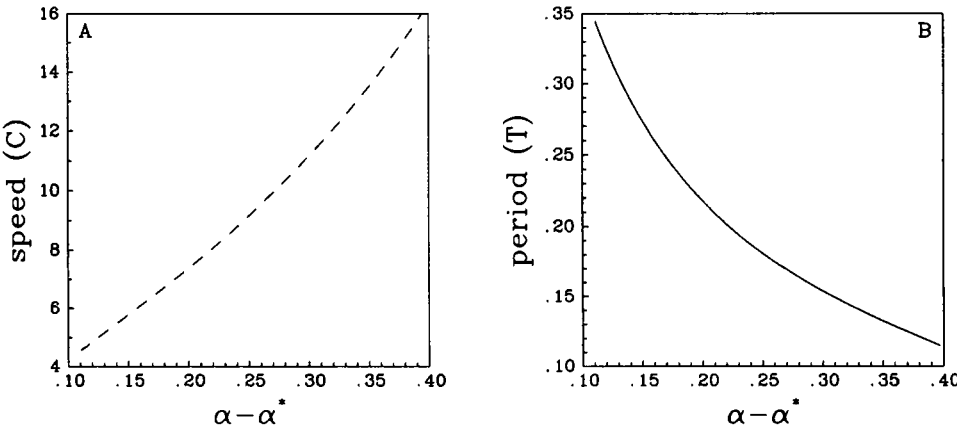


Figure 4 Behavior of speed and period of the MTWs as they approach homoclinicity with the bimodal steady states at $\alpha = \alpha^* = 16.99022$.

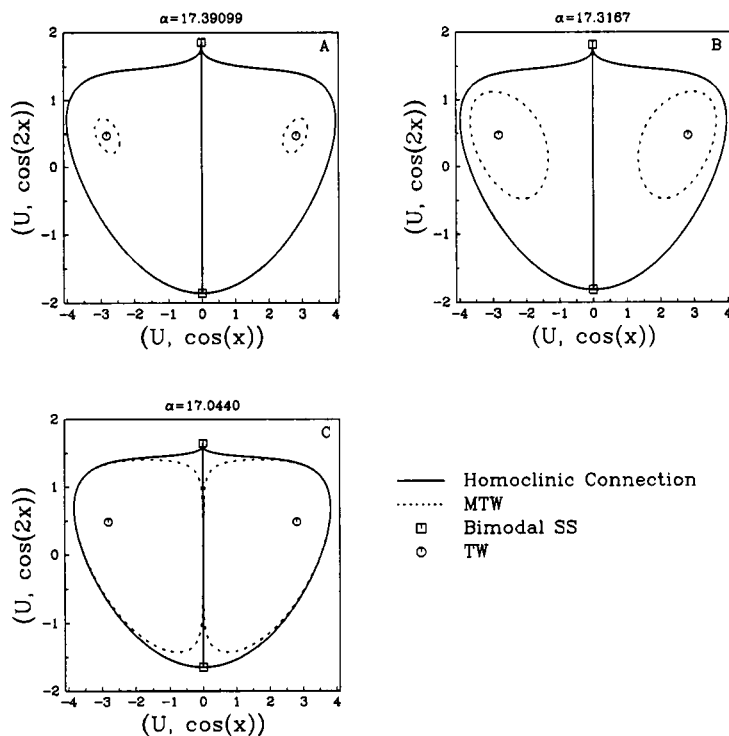


Figure 5 Poincaré section of phase space ($(U, \sin(x)) = 0$) showing MTWs approaching homoclinicity. In this projection, both the left and right running MTWs coincide. The dashed curves are approximations to the torus-plane intersection and were generated by integrating the MTWs through one period. The \circ represent the intersections of the traveling waves with the cutting plane.

observed. The unimodal branch loses stability at $\alpha = 13.005$ to a pair of traveling wave branches, one traveling to the left and one to the right as discussed above (see also Kevrekidis et al. [1990]). This traveling wave branch subsequently loses stability to a subcritical MTW branch at $\alpha \sim 17.400$. The resulting branch of MTW has been approximated on the center-unstable manifold by Armbruster et al. [1989]. They found the bifurcation to be subcritical (in agreement with the computational observations in Kevrekidis et al. [1990]), and showed that, in their approximation, the MTW branch terminated at a persistent heteroclinic loop associated with the bimodal saddle steady states. We were able to switch onto and continue this unstable MTW branch backwards in α . Representative Poincaré maps are shown in Figure 5. As the values of α decrease towards the global bifurcation at $\alpha = 16.99022$, the amplitudes of the Poincaré cuts of the T^2 tori with the $(U, \sin(x)) = 0$ plane are seen to grow. This is much more accurate than the approximate value of 16.8 suggested in Kevrekidis et al. [1990]. These two branches of MTW (and their stable manifolds) provide the separatrix between the stable traveling waves and the stable (attracting) persistent homoclinic loops for $16.99 < \alpha < 17.40$. In this interval, the KSE exhibits hysteretic behavior. Using the arguments of Melbourne et al. [1989], we have computed the lower bounds of the stability interval of the homoclinic connections to be $\alpha = 16.99022$. This computation involved searching along the

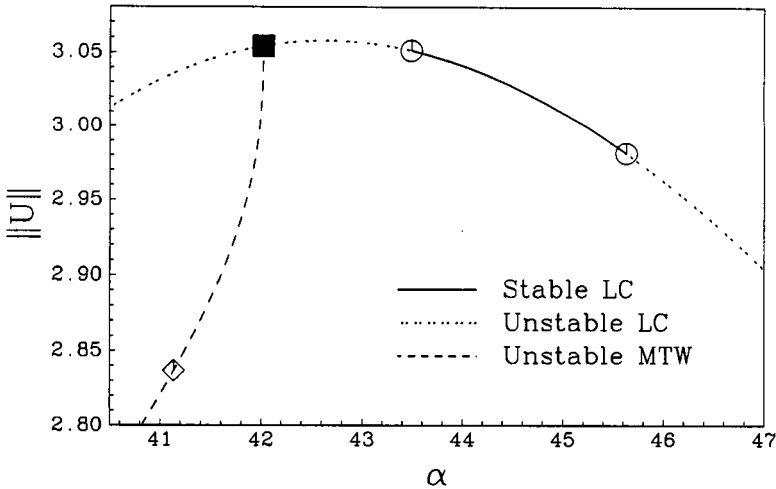


Figure 6 A limit cycle branch giving rise to an MTW branch. LC is an abbreviation for limit cycle and all symbols are defined in Figure 3

bimodal steady state branch for the value of α at which the appropriate eigenvalues had exactly opposite real parts.

After its initial loss of stability at $\alpha = 17.40$, the traveling wave branch is seen in Figure 3A to continue in increasing α and has an additional Hopf bifurcation at $\alpha = 35.050$ giving rise to a new MTW branch. This branch is also born subcritical and never stabilizes; it does undergo a period doubling bifurcation followed by a turning point and another period doubling bifurcation. The fate of this branch will be discussed below.

An alternative bifurcation giving rise to an MTW branch involves the loss of stability of a branch of standing waves (limit cycles) to traveling. Standing waves possess two Floquet multipliers at unity (one because they are limit cycles, the second because of the spatial shift invariance). Such a bifurcation involves an additional Floquet multiplier at unity whose eigenvector becomes aligned with the direction of translational invariance (giving a generalized eigenvector at the bifurcation point). This bifurcation is therefore analogous to the birth of traveling waves from steady states. Such a bifurcation is illustrated in Figure 6.

There are many instances of generation of MTW branches from either traveling wave or standing wave branches in our computations up to $\alpha \approx 95$. This particular example was chosen because of an interesting (but unrelated) bifurcation occurring in its neighborhood. The standing wave branch (which gives rise to the MTW branch at $\alpha \approx 42.02$) has an interval of stability bounded by Hopf bifurcations; a family of T^2 tori is born supercritically at $\alpha \approx 45.03$, and they have been followed by numerical integration up to $\alpha = 45.94$. The Hopf bifurcation at $\alpha = 43.49$ appears to be subcritical.

The MTW branch in Figure 6 is born unstable. An example of a supercritical and stable (observable by integration) MTW branch is shown in Figure 7. A branch of steady states (referred to in the literature as the “Giant” branch Greene and Kim [1988]) bifurcates from the bimodal steady state branch at $\alpha = 52.89$. It becomes stable at $\alpha = 70.04$ in a pitchfork bifurcation to a pair of traveling wave branches (branches not shown) and loses stability via a supercritical Hopf

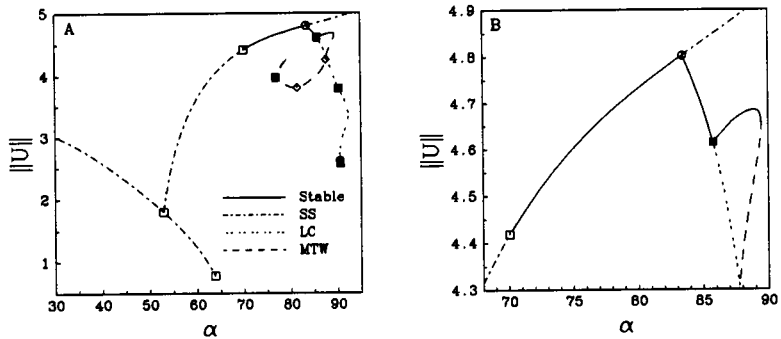


Figure 7 Stable MTW branch bifurcating from a stable standing wave branch. Figure B is a blow up showing detail. In these graphs, and in several that follow, unique styles of dashed lines indicate unstable steady states, limit cycles and modulated traveling waves. Solid lines are used to mark *all* types of stable solutions. All symbols are defined in Figure 3.

bifurcation to stable standing waves at $\alpha = 83.42$. This standing wave branch loses stability to a supercritical (stable) MTW branch at $\alpha = 85.75$. This branch remains stable until $\alpha = 89.48$ when it undergoes a limit point bifurcation and destabilizes. Stable MTW can be observed by simulation in the parameter interval $85.75 < \alpha < 89.48$.

Further Bifurcations of MTW Like limit cycles, stability of MTW can be reported in terms of Floquet multipliers. An MTW solution of (1.1) is stable if the corresponding limit cycle of (1.2) is stable (i.e. has one Floquet multiplier at unity because of the temporal shift invariance, one more multiplier at unity because of the spatial shift invariance, and the remaining multipliers inside the unit circle). In addition to the bifurcations discussed in the previous subsection, involving interaction of MTW with “less complicated” solution types, we find the MTW of the KSE to undergo a number of other bifurcations. Figure 8 compactly illustrates several of these instabilities.

- When a pair of complex Floquet multipliers crosses the unit circle, the MTW branch undergoes a Hopf bifurcation, possibly to a T^3 torus. In Figure 8 this occurs near $\alpha = 55.05$. The resulting attractor is a T^2 torus in a moving frame. This particular bifurcation is supercritical and the resulting T^3 torus is observable by numerical integration (for example, at $\alpha = 55.7$ the coordinate speed is $C = 44.2515$). In Bayliss et al. [1993] such a solution is referred to as a “QPMTW”, a quasiperiodically modulated traveling wave.
- When a Floquet multiplier crosses the unit circle through -1 , a period doubling occurs. Shown in Figure 8 are several such period doublings. A subcritical period doubling occurs at $\alpha = 55.87$, with subsequent period doublings at $\alpha = 55.71$ to a “period 4” MTW, and of this latter branch to a “period 8” MTW (not shown in the figure) at $\alpha = 55.73$. We believe that a full period doubling cascade follows.
- At a limit point bifurcation, a Floquet multiplier crosses the unit circle at 1. An example of this is seen in Figure 8 where the subcritical period 2 MTW branch turns and becomes stable at $\alpha = 55.7078$.

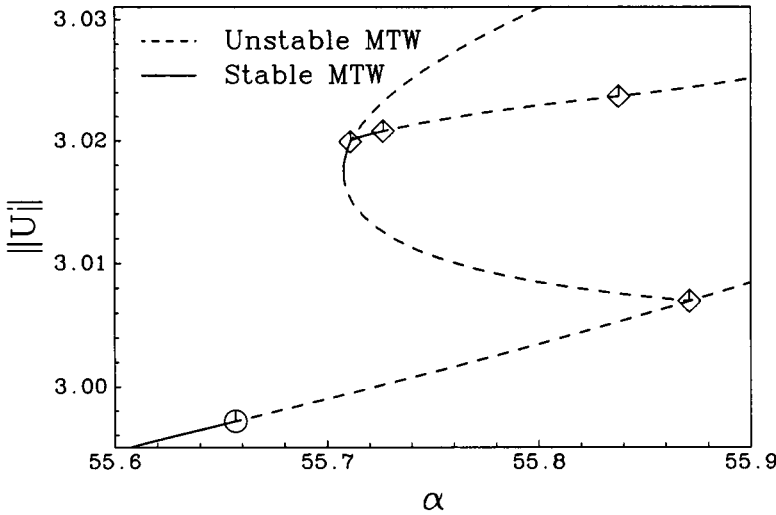


Figure 8 KSE bifurcation diagram showing a limit point, a Hopf bifurcation, and several period doublings of MTW. All symbols are defined in Figure 3.

These bifurcations appear analogous to those of generic limit cycles; for example, the traveling wave to MTW bifurcation is analogous to the regular Hopf bifurcation, and the period doubling of MTW is analogous to regular period doubling. There is a distinction, however, since not only the amplitude and period of the various branches change with the bifurcation parameter α ; the traveling speed, C , also varies with α . Figure 9A shows the variation of both the period and speed of the “period 2” MTW branch close to the period doubling bifurcation at $\alpha = 55.87$ in Figure 8 (enlarged in Figure 9B). Figure 10A shows the corresponding asymptotic behavior of the period and speed of an MTW branch with respect to α in the neighborhood of a Hopf bifurcation from a traveling wave branch ($\alpha = 52.85$) enlarged in Figure 10B.

Figure 11 shows a bifurcation diagram including various MTW branches and their bifurcations, computed with a 9 mode Fourier spectral discretization. For all its complexity, the bifurcation diagram is still partial, and a number of features in it remain unresolved. For example, in Figure 12 a branch of MTW is seen to approach the neighborhood of a singular point (triple zero eigenvalue) on the trimodal steady state branch at $\alpha = 36.235$. While the symmetry breaking steady state bifurcations in the neighborhood of such a point have been studied (Krupa [1988, 1990]), the local *dynamics* have not been completely described.

Symmetric MTW It can be shown that if a k -modal steady state (traveling wave) branch has a Hopf bifurcation at $\alpha = \alpha^*$ while its unimodal “parent” does not have one at $\alpha = \alpha^*/k^2$, then the limit cycle (MTW) branch born at the Hopf bifurcation point will have the following property:

$$U(x, t) = U\left(x + \frac{2\pi}{k}, t + \frac{T}{k}\right) \quad (4.1)$$

T here is the period of the oscillation and the MTW is assumed to be in the “proper” traveling frame so as to appear as a limit cycle for equation (1.2). Limit

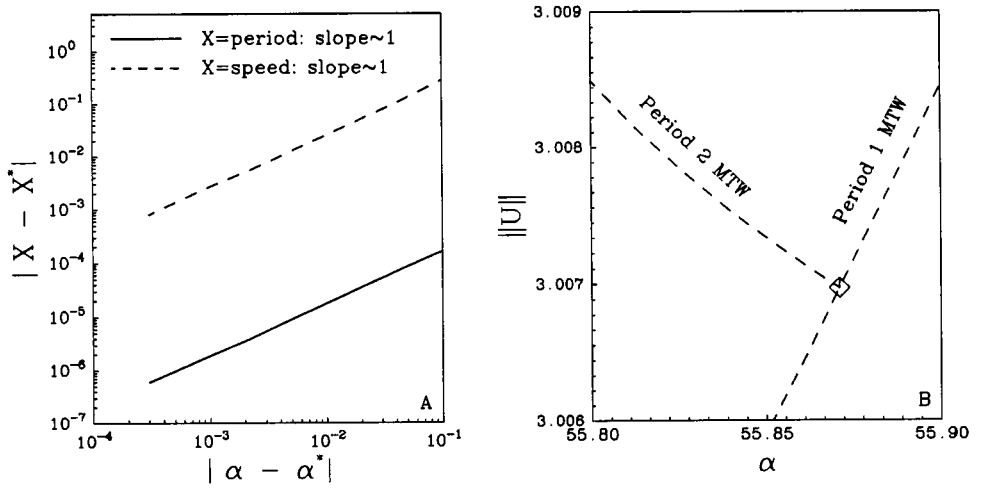


Figure 9 Asymptotic behavior near a period doubling bifurcation of MTW. The "*" superscript denotes values at the period doubling bifurcation point ($\alpha^* = 55.87$).

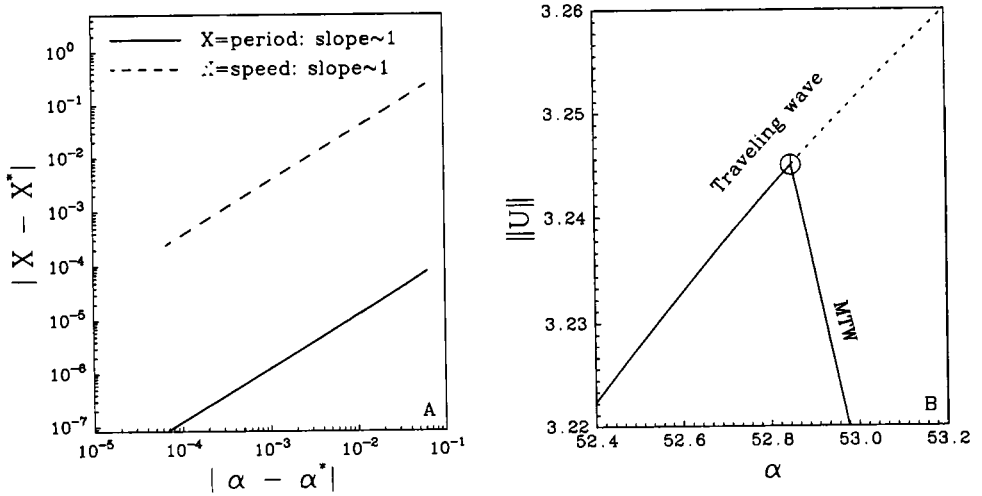


Figure 10 Asymptotic behavior after the birth of an MTW branch from a Hopf bifurcation of a traveling wave branch. The "*" superscript denotes values at the Hopf bifurcation point ($\alpha^* = 52.85$).

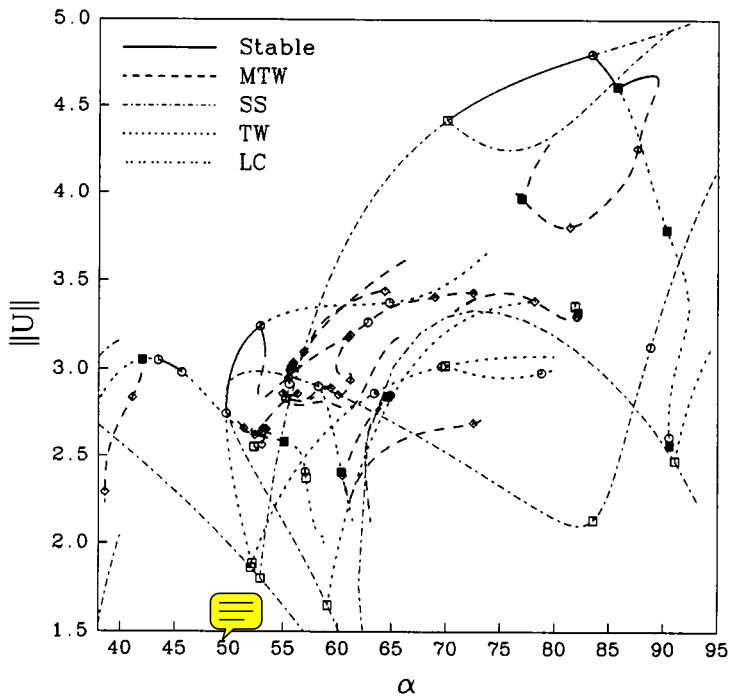


Figure 11 Bifurcation diagram containing all computed MTWs in the parameter interval $38 < \alpha < 95$. Solid lines indicate stable solutions as described in Figure 12. Symbols and abbreviations are defined in Figure 3.

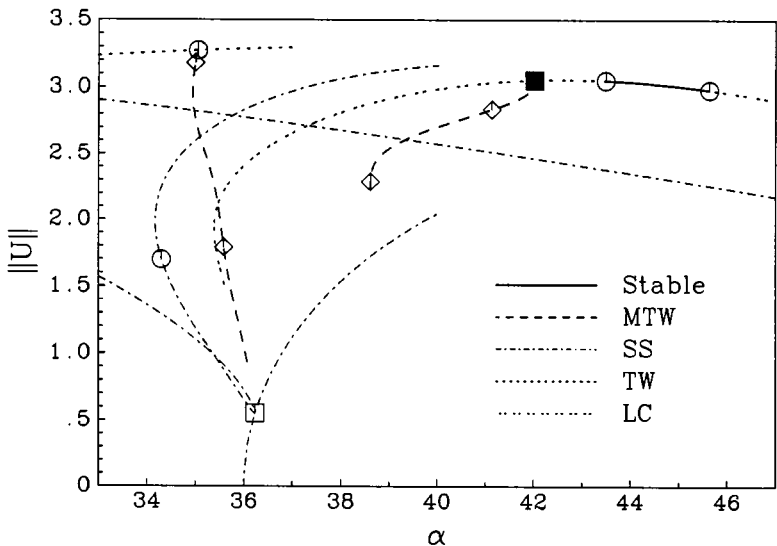


Figure 12 Behavior near a triple zero singular point on the trimodal steady state branch. All solutions are unstable except for those in the solid portion of the limit cycle branch. All symbols and abbreviations are defined in Figure 3.

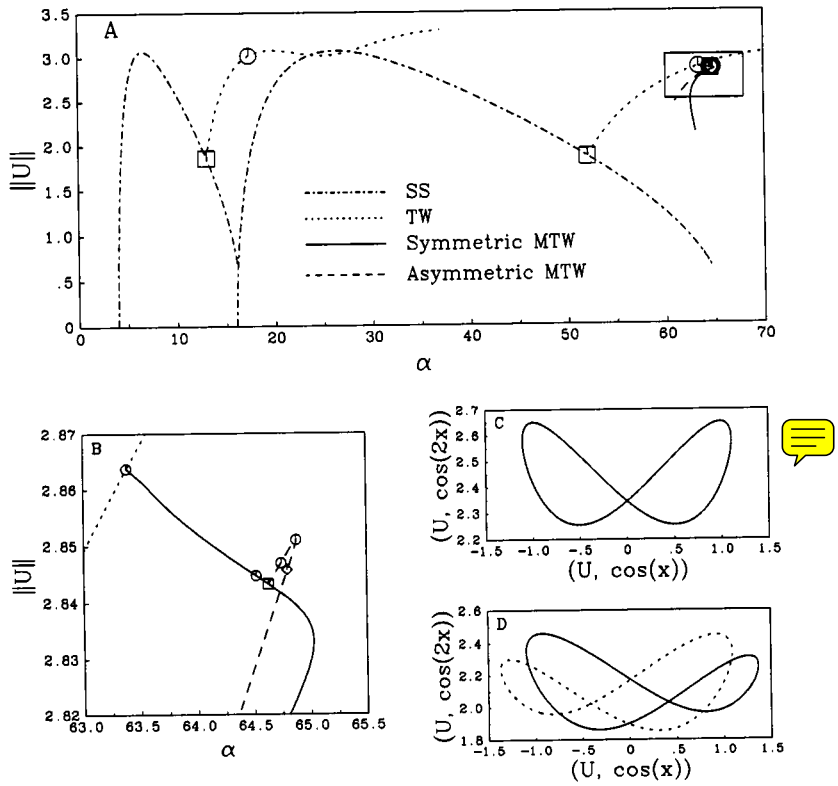


Figure 13 A) Unimodal and bimodal steady state, traveling wave, and MTW branches (stability not indicated). B) Blow up showing symmetric MTW bifurcating to asymmetric MTW. C) Phase space projection of a symmetric MTW and D) Phase space projections of an asymmetric MTW and its spatial π shift (dashed) in the traveling frame.

cycles possessing this type of symmetry (sometimes called “ponies on a merry-go-round” (Aronson et al.[1991])) are known to suppress period doubling in generic one parameter systems (Swift and Wiesenfeld [1984]). Instead, the symmetric solution may first undergo a pitchfork bifurcation to a pair of asymmetric (symmetric to each other) solutions, which may then subsequently period double. Figure 13 illustrates this situation for a symmetric MTW which bifurcates from a bimodal traveling wave at $\alpha = 63.3826$. Note that the unimodal traveling wave branch has its first Hopf at $\alpha = 17.3998$ which predicts the bimodal replica Hopf at $\alpha = 2^2 \cdot 17.3998 = 69.5992$. Since the bimodal Hopf at $\alpha = 63.3826$ is not a replica of any unimodal Hopf, we know *a priori* that the emanating MTW branch must have the symmetry described in equation (4.1) (with $k = 2$). As expected, this MTW branch does not period double directly. Instead, it has a pitchfork bifurcation at $\alpha = 64.6283$ and the resulting asymmetric pair of MTW subsequently period doubles at $\alpha = 64.7947$ (see enlargement in Figure 13B). Note also that both the symmetric and asymmetric MTW undergo Hopf bifurcations in this parameter range.

5 Summary and Discussion

We presented an algorithm for the computation of MTW in nonlinear evolution PDEs with periodic boundary conditions in one spatial dimension. We illustrated the use of the algorithm by computing several MTW branches and their bifurcations (both global and local) for the Kuramoto–Sivashinsky equation. These branches of MTW play an important role in the development of spatiotemporal patterns and eventually chaotic behavior in the KSE. The algorithm reduces the computation of an MTW to a set of coupled nonlinear algebraic equations. Standard pseudo-arclength techniques were used to continue these solutions in parameter space. Since, however, it is important to study the MTW branches in relation to other types of solutions of the PDE (traveling waves, standing waves), branch switching between different type solution branches becomes an important consideration. As we point out in the appendix, the type of phase pinning condition chosen allows the use of standard branch switching techniques for steady states and limit cycles of generic ODEs in our problem. We actually used the ODE branch switching algorithms in AUTO (Doedel [1981, 1986]) for all of the branch switching calculations in this paper.

As shown in Appendix A, for our choice of pinning conditions there is a direct and simple relation between the state transition matrix for a limit cycle of the PDE and the Jacobian of equation (2.4) (an $(M+2) \times (M+2)$ matrix). The state transition matrix Γ is the $M \times M$ matrix:

$$\Gamma \equiv \frac{\partial \vec{a}(t=T)}{\partial \vec{a}(t=0)}.$$

The upper left $M \times M$ block of the Jacobian of the inflated system (2.4) is $\Gamma - I$.

Solutions of equation (2.4) correspond to MTW of the original PDE (1.1). For general pinning conditions, one does not expect the $M+2$ eigenvalues of the Jacobian of (2.4) to relate to the M eigenvalues of $\Gamma - I$. For the pinning conditions described above, the relation is as follows: The 2 matrices share $M-2$ eigenvalues; the remaining 2 eigenvalues of $\Gamma - I$ are lost; these were equal to zero, since Γ had two eigenvalues at unity. Depending on whether the pinned extremum is a minimum or a maximum, the 4 additional eigenvalues of the Jacobian are found to be:

$$\lambda = \pm \sqrt{\frac{1}{2} \left\{ (TU_{xx} + U_{tt}) \pm \sqrt{(TU_{xx} + U_{tt})^2 - 4T(U_{xx}U_{tt} - U_{xt}^2)} \right\}}_{x=t=0}.$$

This formula is derived in a more general setting in Appendix A. It is therefore possible to monitor the stability of the MTW branch (quantified by the eigenvalues of Γ) by monitoring the eigenvalues of the Jacobian and ignoring the 4 nonrelevant eigenvalues. This allows the detection of not only turning points and pitchfork bifurcations (which in general can be detected by inflated systems) but also of Hopf bifurcations and period doublings.

In our calculations, we used the switching subroutines in the continuation package AUTO (Doedel [1981, 1986]), for the “bogus” inflated dynamical system:

$$\begin{aligned} \ddot{\vec{a}} &= g(\vec{a}, C; \alpha) \\ \dot{C} &= P_1(\vec{a}) = 0. \end{aligned} \tag{5.1}$$

All relevant types of solution of the original PDE (1.1) (steady states, traveling waves, standing waves, and MTW) and their bifurcations correspond to solutions and bifurcations of this “bogus” dynamical system of ODEs. Steady states of the PDE are steady states of (5.1) with $C = 0$. Traveling waves of the PDE are steady states of (5.1) with $C \neq 0$. Limit cycles of the PDE (MTW) are limit cycles of (5.1) with $C = 0$ ($C \neq 0$ respectively). The inflated system exhibits a regular Hopf bifurcation when a traveling wave loses stability to an MTW, and AUTO is therefore capable of switching directly onto MTW branches.

Although stable MTWs have been observed for PDEs in several contexts via numerical integration, few references address their computation via a fixed point method. Soibelman [1989] and Soibelman and Meiron [1991] continued stable and unstable 2 dimensional (in space) MTWs in their study of bifurcations in plane Poiseuille flow. They report that bifurcations of MTWs were observed by numerical integration but that stability of MTWs was not computed because of the prohibitive memory requirements of the method used. For a one dimensional problem, their method would involve expanding *both* the spatial and temporal directions in Fourier series:

$$U(x, t) = \sum_{n=-N}^N \sum_{m=-M}^M a_{n,m} e^{inx} e^{imt}$$

and solving for the $\approx 4NM$ coefficients using Newton’s method. The problem inherent in expanding the temporal dimension is that sharp oscillations, (for example as a MTW branch approaches homoclinicity) are not well represented by a short truncation of a Fourier series. Large M is required to accurately resolve temporal oscillations. The Jacobian matrix would require $O(N^2 M^2)$ memory locations which can become costly as M will generally be large—possibly in the hundreds for the accurate resolution of MTWs nearing homoclinicity. The memory problems of course become more significant for the two (space) dimensional PDE they considered. In contrast, the algorithm presented here uses a traditional spatial discretization with a *shooting* algorithm in time and requires only $O(N^2)$ memory locations (for the Jacobian) to accurately resolve the temporal oscillations. With K shooting points, $O(KN^2)$ memory locations are required.

In their study of binary fluid convection, Knobloch and Moore [1990] computed stable MTW using both numerical integration and a fixed point method. Their fixed point method, like that of Soibelman and Meiron, involved Fourier expanding the temporal dependence. They observed MTW arising from bifurcations of both traveling waves and limit cycles. They also reported the global bifurcation behavior of MTW in the neighborhood of a Takens–Bogdanov point.

We expect that the shooting formulation presented here (along with the “tricks” that allow the use of standard bifurcation/continuation software for steady states and limit cycles) will be useful in computer assisted studies of MTWs for a large class of discretized PDEs. In particular, it could help elucidate the role of unstable MTWs in global bifurcations.

Acknowledgements

This work was partially supported by the National Science Foundation and by the David and Lucile Packard Foundation. Most of it was part of (and has been published in) the Ph.D. thesis of one of the authors (HSB) Brown [1992].

References

- Adomaitis, R. and Abed, E. [1992], *Bifurcation analysis of nonuniform flow patterns in axial-flow bas compressors*, Technical Report TR 92-121, Systems Research Center, U. Maryland.
- Armbruster, D., Guckenheimer, H. and Holmes, P. [1988], *Heteroclinic cycles and modulated travelling waves in systems with $O(2)$ symmetry*, *Physica D*, **29**, 257-282.
- Armbruster, D., Guckenheimer, J. and Holmes, P. [1989], *Kuramoto-Sivashinsky dynamics on the center-unstable manifold*, *SIAM J. Appl. Math.*, **49(3)**, 676-691.
- Aronson, D.G., Golubitsky, M. and Mallet-Paret, J. [1991], *Ponies on a merry-go-round in large arrays of Josephson junctions*, *Nonlinearity*, **4**, 903-910.
- Atherton, R.W. and Homsy, G.M. [1976], *On the derivation of evolution equations for interfacial waves*, *Chemical Engineering Communications*, **2**, 57-77.
- Bayliss, A., Matkowsky, B.J. and Riecke, H. [1992], *Modulated traveling waves in combustion*, in H. G. Kaper and M. Garbey, editors, *Numerical Methods for PDEs With Critical Parameters*, 137-162. Kluwer, Dordrecht.
- Bayliss, A., Matkowsky, B.J. and Riecke, H. [1993], *Structure and dynamics of modulated traveling waves in cellular flames*, Preprint.
- Benney, D.J. [1966], *Long waves on liquid films*, *Journal of Mathematical Physics*, **45**, 150-155.
- Brown, H.S. [1992], *A Computer Assisted, Nonlinear Dynamic Study of Instabilities and Pattern Formation for Interfacial Waves*, PhD thesis, Princeton University.
- Brown, H.S., Kevrekidis, I.G. and Jolly, M.S. [1991], *A minimal model for spatio-temporal patterns in thin film flow*, in H. Swinney, R. Aris, and D. Aronson, editors, *Patterns and Dynamics in Reactive Media*, **37**, IMA Volumes in Mathematics and its Applications, Springer.
- Doedel, E. [1981], *AUTO: a program for the automatic bifurcation analysis of autonomous systems*, *Cong. Num.*, **30**, 265-284.
- Doedel, E. [1986], *Auto 86 User Manual*, CalTech, Pasadena.
- Greene, J. and Kim, J.-S. [1988], *The steady states of the Kuramoto-Sivashinsky equation*, *Physica D*, **33**, 99-120.
- Iooss, G. [1993], *Bifurcation from group orbits of solutions*, Private communication.
- Keller, H.B. [1976], *Numerical Solution of Two Point Boundary Value Problems*, SIAM.
- Kevrekidis, I., Aris, R., Schmidt, L. and Pelikan, S. [1985], *Numerical computations of invariant circles of maps*, *Physica D*, **16**, 243-251.
- Kevrekidis, I., Nicolaenko, B. and Scovel, J. [1990], *Back in the saddle again: A computer assisted study of the Kuramoto-Sivashinsky equation*, *SIAM Journal of Applied Math.*, **50(3)**, 760-790.

- Knobloch, E. and Moore, D. [1990], *Minimal model of binary fluid convection*, Phys. Rev. A, **42(8)**, 4693-4709.
- Krupa, M. [1988], *Bifurcations of Critical Group Orbits*, PhD thesis, University of Houston.
- Krupa, M. [1990], *Bifurcations of relative equilibria*, SIAM J. Math. Anal., **21(6)**, 1453-1486.
- Melbourne, I., Chossat, P. and Golubitsky, M. [1989], *Heteroclinic cycles involving periodic solutions in mode interactions with $O(2)$ symmetry*, Proc. Royal Soc. Edinburgh, **113A**, 315-345.
- Rand, D. [1982], *Dynamics and symmetry, predictions for modulated waves in rotating fluids*, Arch. Rational Mech. An., **79**, 1-37.
- Scovel, J.C., Kevrekidis, I.G. and Nicolaenko, B. [1988], *Scaling laws and the prediction of bifurcations in systems modeling pattern formation*, Physics Letters A, **130**, 73-80.
- Sivashinsky, G.I. and Michelson, D.M. [1980], *On irregular wavy flow of a liquid down a vertical plane*, Prog. Theor. Phys., **63**, 2112-2114.
- Soibelman, I. [1989], *A Study of Finite Amplitude Bifurcations in Plane Poiseuille Flow*, PhD thesis, California Institute of Technology.
- Soibelman, I. and Meiron, D.I. [1991], *Finite-amplitude bifurcations in plane Poiseuille flow: two-dimensional Hopf bifurcation*, Journal of Fluid Mechanics, **229**, 389-416.
- Swift, J.W. and Wiesenfeld, K. [1984], *Suppression of period doubling in symmetric systems*, Phys. Rev. Letters, **52(9)**, 705-708.
- van Veldhuizen, M. [1987], *A new algorithm for the numerical approximation of an invariant curve*, SIAM J. Sci. St. Comp., **8(6)**, 951-962.

Appendix A Inflated Jacobians and Stability.

Let $U(x, t)$ be a limit cycle of a PDE: $U_t = F(U)$ with periodic boundary conditions: $U(x, t) = U(x + 2\pi, t)$. Stability of limit cycles is reported in terms of eigenvalues of the state transition matrix: $\Gamma \equiv \frac{\partial U(T)}{\partial U(0)}$ which has two eigenvalues fixed at 1. These correspond to the two perturbations, U_t and U_x , that remain on the limit cycle due to translational invariance in both time and space. To eliminate these invariances, two phase pinning constraints are imposed and the system is inflated as discussed previously. As a result of the inflation process, the following Jacobian matrix arises in the (Newton) iterative computation of MTW:

$$J \equiv \begin{bmatrix} \frac{\partial U(t=T)}{\partial U(t=0)} & \frac{\partial U(T)}{\partial C} & \frac{\partial U(T)}{\partial T} \\ P_1 & 0 & 0 \\ P_2 & 0 & 0 \end{bmatrix}. \quad (\text{A.1})$$

Here we address the question of obtaining information about MTW stability from this inflated matrix J . The eigenvalues of this matrix do indeed contain the stability information of the correct matrix Γ and hence continuation schemes based on the inflated system will correctly report bifurcations of MTW. While what follows is motivated by the MTW problem it is, however, more general.

Let L be an operator with known spectrum: $L\phi_j = \eta_j\phi_j$ and assume, for simplicity, that L has non-repeated, real eigenvalues with the possible exception that $\eta_1 = \eta_2$. We wish to establish a connection between the eigenvalues, η , of L and the eigenvalues, λ , of J :

$$J\vec{v}_m \equiv \begin{bmatrix} L & \phi_1 & \phi_2 \\ P_1 & 0 & 0 \\ P_2 & 0 & 0 \end{bmatrix} \begin{bmatrix} v_m \\ k_{1,m} \\ k_{2,m} \end{bmatrix} = \lambda_m \begin{bmatrix} v_m \\ k_{1,m} \\ k_{2,m} \end{bmatrix} \quad (\text{A.2})$$

where:

$$\begin{aligned} \phi, v &\in L^2 \\ k_1, k_2, \lambda, \eta &\in \mathbb{R} \\ L : L^2 &\rightarrow L^2 \\ P_1, P_2 : L^2 &\rightarrow \mathbb{R}. \end{aligned}$$

Equation (A.2) is equivalent to:

$$(L - \lambda_m)v_m + k_{1,m}\phi_1 + k_{2,m}\phi_2 = 0 \quad (\text{A.3})$$

$$P_1 v_m = \lambda_m k_{1,m} \quad (\text{A.4})$$

$$P_2 v_m = \lambda_m k_{2,m}. \quad (\text{A.5})$$

Expand the function v_m in the eigenfunction basis so that: $v_m = \sum_{n=1}^{\infty} a_{n,m}\phi_n$ and substitute into (A.3):

$$0 = \phi_1 [k_{1,m} + (\eta_1 - \lambda_m)a_{1,m}] + \phi_2 [k_{2,m} + (\eta_2 - \lambda_m)a_{2,m}] + \sum_{n=3}^{\infty} (\eta_n - \lambda_m)a_{n,m}\phi_n. \quad (\text{A.6})$$

Since the ϕ 's are linearly independent, the series must vanish termwise and (A.6) is satisfied only if:

$$0 = k_{1,m} + (\eta_1 - \lambda_m)a_{1,m} \quad (\text{A.7})$$

$$0 = k_{2,m} + (\eta_2 - \lambda_m)a_{2,m} \quad (\text{A.8})$$

$$0 = (\eta_n - \lambda_m)a_{n,m} \quad n \geq 3. \quad (\text{A.9})$$

Clearly a nontrivial solution to equation (A.9) is:

$$\lambda_m = \eta_m, \quad (m \geq 3) \quad a_{n,m} = \begin{cases} 0 & \text{if } n \neq m, m \geq 3 \\ \text{arbitrary} \equiv 1 & \text{if } n = m, m \geq 3. \end{cases}$$

Equations (A.7) and (A.8) can now be solved for $a_{1,m}$ and $a_{2,m}$:

$$a_{1,m} = \frac{-k_{1,m}}{(\eta_1 - \eta_m)} \quad a_{2,m} = \frac{-k_{2,m}}{(\eta_2 - \eta_m)}$$

and we see that v_m takes on the general form: $v_m = \phi_m + a_{1,m}\phi_1 + a_{2,m}\phi_2$, ($m \geq 3$.) When $m = 1$ or $m = 2$, equation (A.9) indicates that for $n \geq 3$: $a_{n,1} = a_{n,2} = 0$ and v_1 and v_2 take on the form: $v_m = a_{1,m}\phi_1 + a_{2,m}\phi_2$, ($m = 1, 2$.) Substituting this into (A.4) and (A.5) and solving for the k 's gives:

$$k_{1,1} = \frac{a_{1,1}P_1\phi_1 + a_{2,1}P_1\phi_2}{\lambda_1} \quad k_{2,1} = \frac{a_{1,1}P_2\phi_1 + a_{2,1}P_2\phi_2}{\lambda_1}.$$

When these are substituted into (A.7) and (A.8) the linear system arises:

$$\begin{bmatrix} \frac{P_1\phi_1}{\lambda_1} + (\eta_1 - \lambda_1) & \frac{P_1\phi_2}{\lambda_1} \\ \frac{P_2\phi_1}{\lambda_1} & \frac{P_2\phi_2}{\lambda_1} + (\eta_2 - \lambda_1) \end{bmatrix} \begin{bmatrix} a_{1,1} \\ a_{2,1} \end{bmatrix} = \begin{bmatrix} 0 \\ 0 \end{bmatrix}.$$

Nontrivial solutions exist only when the determinant is zero:

$$\begin{aligned} 0 &= \left[\frac{P_1\phi_1}{\lambda_1} + (\eta_1 - \lambda_1) \right] \left[\frac{P_2\phi_2}{\lambda_1} + (\eta_2 - \lambda_1) \right] - \left(\frac{P_1\phi_2}{\lambda_1} \right) \left(\frac{P_2\phi_1}{\lambda_1} \right) \\ &= [P_1\phi_1 + \lambda_1(\eta_1 - \lambda_1)][P_2\phi_2 + \lambda_1(\eta_2 - \lambda_1)] - P_1\phi_2 P_2\phi_1. \end{aligned} \quad (\text{A.10})$$

This is a fourth order polynomial in λ_1 whose roots are the missing eigenvalues. The same polynomial arises for $m = 2$. All four eigenvalues will be observed since we have not only "lost" two of L 's eigenvalues but also need two additional eigenvalues as a result of inflating the system. When $\eta_1 = \eta_2$ the roots of (A.10) are particularly easy to write. This case is relevant because when computing modulated traveling waves, $\eta_1 = \eta_2 = 1$. Letting $W \equiv \lambda_1(\lambda_1 - \eta_1)$ transforms (A.10) into a second order polynomial in W :

$$W^2 - W(P_1\phi_1 + P_2\phi_2) + (P_1\phi_1 P_2\phi_2 - P_1\phi_2 P_2\phi_1) = 0$$

with roots:

$$W = \frac{1}{2} \left\{ (P_1\phi_1 + P_2\phi_2) \pm \sqrt{(P_1\phi_1 + P_2\phi_2)^2 - 4(P_1\phi_1 P_2\phi_2 - P_1\phi_2 P_2\phi_1)} \right\}. \quad (\text{A.11})$$

The λ 's are recovered by solving: $\lambda_1^2 - \lambda_1 \eta_1 - W = 0$ to obtain:

$$\lambda_1 = \frac{1}{2} \left\{ \eta_1 \pm \sqrt{\eta_1^2 + 4W} \right\}.$$

Example 1: Modulated Traveling Waves As discussed in section 2, L will have two eigenvalues $\eta_1 = \eta_2 = 1$ with eigenfunctions $U_x(t=0)$ and $U_t(t=0)$. With the shooting scheme used, it is straightforward to show that upon convergence to a MTW,

$$\begin{aligned} \phi_1 &\equiv \frac{\partial U(T)}{\partial C} = TU_x(t=T) = TU_x(t=0) \\ \phi_2 &\equiv \frac{\partial U(T)}{\partial T} = U_t(t=T) = U_t(t=0) \end{aligned}$$

If the phase is pinned so that an extremum of the surface, $U(x, t)$ is at the origin ($U_x(x=t=0) = U_t(x=t=0) = 0$) then $P_1 \equiv \partial_x|_{x=t=0}$ and $P_2 \equiv \partial_t|_{x=t=0}$. Of the $N+2$ eigenvalues of the augmented system, $N-2$ of them are the same as those for L . The pair of eigenvalues that were at 1 for L are, as predicted above, not observed. The 4 “missing” eigenvalues are recovered by applying (A.11) and (A.4):

$$W = \frac{1}{2} \left\{ (U_{xx} + U_{tt}) \pm \sqrt{(U_{xx} + U_{tt})^2 - 4T(U_{xx}U_{tt} - U_{xt}^2)} \right\}_{x=t=0} \quad (\text{A.12})$$

$$\lambda = \frac{1 \pm \sqrt{1 + 4W}}{2}. \quad (\text{A.13})$$

Traveling Wave Computation When computing traveling waves it is only necessary to inflate by one equation and the analysis is simpler than for MTW. The eigenvalue problem for traveling wave Jacobians is:

$$J\vec{v}_m \equiv \begin{bmatrix} L & \phi_1 \\ P_1 & 0 \end{bmatrix} \begin{bmatrix} v_m \\ k_m \end{bmatrix} = \lambda_m \begin{bmatrix} v_m \\ k_m \end{bmatrix}. \quad (\text{A.14})$$

It is straightforward to show that the eigenfunctions will take the form: $v_m = \phi_m + C_m \phi_1$ and all but one of L 's eigenvalues will be eigenvalues of J ; that is $\lambda_m = \eta_m$ except when $m = 1$. When $m = 1$, the eigenfunction is: $v_1 = \phi_1$. Applying a solvability argument, the missing eigenvalue (λ_1) and the additional one due to inflating are found to be the roots of the quadratic equation:

$$\lambda^2 - \lambda \eta_1 - P_1 \phi_1 = 0 \quad \longrightarrow \quad \lambda = \frac{1}{2} \left[\eta_1 \pm \sqrt{\eta_1^2 + 4P_1 \phi_1} \right]$$

For traveling wave computations, we are especially interested in the case $\eta_1 = 0$ and thus:

$$\lambda = \pm \sqrt{P_1 \phi_1}.$$

Depending on the sign of $P_1 \phi_1$, three distinctly different cases arise: (a) $P_1 \phi_1 > 0$; A pair of real eigenvalues that are equal in magnitude and opposite in sign, (b) $P_1 \phi_1 = 0$; A pair of zero eigenvalues, and (c) $P_1 \phi_1 < 0$; A pair of purely imaginary eigenvalues:

$$\lambda = \pm i \sqrt{|P_1 \phi_1|} \equiv \pm i \omega.$$

Example 2: Traveling Waves Let U be an M dimensional approximation of the PDE $U_t = F(U)$. Computation of traveling waves involves finding steady states of the augmented system:

$$U_t = F(U) + CU_x \equiv G(U, C).$$

For solutions with imposed spatially periodic boundary conditions, the $M \times M$ Jacobian (evaluated at the traveling wave), $\frac{\partial G}{\partial U} \equiv L$, has the null vector U_x corresponding to translational invariance. As with MTW, an extremum is usually pinned at the origin:

$$P_1 U = U_x(x=0) = 0; \quad P_1 \equiv \partial_x|_{x=0}.$$

The resulting $(M+1) \times (M+1)$ system has the Jacobian:

$$J = \begin{bmatrix} L & \frac{\partial G}{\partial C} \\ \frac{\partial P_1}{\partial U} & \frac{\partial P_1}{\partial C} \end{bmatrix} = \begin{bmatrix} L & U_x \\ \partial_x|_{x=0} & 0 \end{bmatrix}.$$

This matrix now takes the form of (A.14), and as shown above, J 's eigenvalues will be the same as those of L except for the missing $\lambda = 0$. The two remaining eigenvalues are expected to be: $\lambda = \pm \sqrt{U_{xx}(x=0)}$. Problems occur when $U_{xx}(x=0) < 0$ and a purely imaginary pair arises. With a pair of eigenvalues always lying on (practically very close to) the imaginary axis, continuation programs like AUTO will constantly detect spurious Hopfs. When a "true" Hopf occurs, it will be difficult to distinguish between the "true" crossing pair of eigenvalues and the pair hovering around the imaginary axis. Numerical roundoff errors often cause this "fixed" pair to jump from one side of the imaginary axis to the other. The real parts might vary between say -10^{-9} and 10^{-9} which is effectively zero; nevertheless a sign change signaling a Hopf bifurcation will be detected.

The "complex extra eigenvalue pair" case arises when the solution at $x=0$ is a maximum ($U_{xx}(0) < 0$); the "two real eigenvalues" case arises when the solution is a minimum ($U_{xx}(0) > 0$). This information is useful because it shows that the continuation of traveling waves should have no problems detecting Hopf bifurcations provided the pinned extremum is a minimum.